Engineering Science & Technology
https://ojs.wiserpub.com/index.php/EST/

UNIVERSAL WISER PUBLISHER

Research Article

# Wind-Induced Dynamic Behavior of Mechanically Attached Single-Ply Membrane Roofing Systems Installed on Flat Roofs

**Yasushi Uematsu[1*], Shingo Sugiyama[2], Takuto Usukura[3]**

[1]National Institute of Technology (KOSEN), Akita College, Akita, Japan
[2]Taisei Corporation, Tokyo, Japan
[3]Tajima Roofing Inc., Tokyo, Japan
Email: uematsu@akita-nct.ac.jp

**Received:** 29 June 2021; **Revised:** 31 August 2021; **Accepted:** 8 September 2021

**Abstract:** The present paper investigates the wind-induced dynamic behavior of a mechanically attached single-ply membrane roofing system installed on flat roofs of middle-rise and high-rise buildings, with or without parapets. First, the wind pressure distributions on the roof were measured in a turbulent boundary layer. The results indicate that the parapets affect the wind pressure distributions significantly. Very large peak suctions are induced near the windward corner of the roof under oblique wind conditions in the case of a building without parapets. Then, we developed a test method for evaluating the wind-resistant performance of the roofing system using three Pressure Loading Actuators (PLAs) and a chamber to which a full-scale specimen was attached. In the experiments, the chamber was divided into three spaces using thin silicon sheets. The PLAs generated different fluctuating pressures in these spaces using the time history of wind pressure coefficients measured at three points near the windward corner of the roof in an oblique wind. We measured the membrane deformations and the wind forces acting on the fasteners connecting the membrane to the structural substrate. The results indicate that horizontal forces nearly equal to or larger than the vertical ones are generated on the fasteners, which may cause pulling out of fasters more easily. The failure mode was found to be different from that obtained from a ramped pressure loading test. We have also developed a model of finite element analysis, which was validated by an experiment. The results of analysis for a wide area of roofing system indicate that relatively large horizontal forces may be generated on the fasteners in the field region of the roof for buildings with parapets.

***Keywords*:** mechanically attached single-ply membrane roofing system, wind-resistant performance, wind tunnel experiment, pressure loading actuator, full-scale roofing assembly, finite element analysis

## 1. Introduction

Mechanically attached single-ply membrane roofing systems are often used for flat roofs because of their high work ability, low installation cost, and consideration for environmental conservation. In this system, the waterproofing membrane is fixed to the roof substrate with a series of fasteners. Figure 1 shows a typical construction method used for steel structures in Japan. The fasteners are arranged in a square lattice-like form with a spacing of 0.45-1.0 m (typically 0.6 m). This method is somewhat different from that generally used in Europe and North America where the membranes


DOI: https://doi.org/10.37256/est.3120221019

are anchored to the roof substrate at many points along the seams of membranes. In any case, wind-induced suction lifts the membrane between the attachments and causes membrane billowing and elongation. The roofing systems are so sensitive to dynamic wind actions that they are often damaged by strong winds, particularly near the roof corner where high suctions are induced by conical vortices in oblique winds [1]. High billowing of the membrane due to strong winds may cause tear of membrane or pull-out of fasteners [2]. Therefore, wind-resistant performance is one of the greatest concerns for structural engineers when designing this type of roofing system.

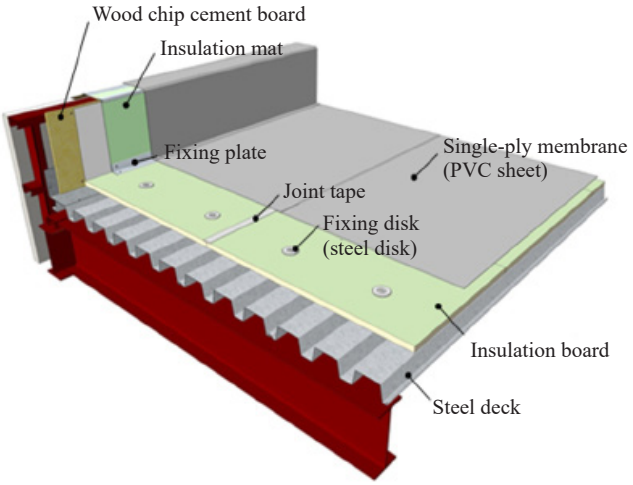


**Figure 1.** Schematic illustration of mechanically-attached single-ply membrane roofing system used in Japan

For the safe design, it is important to appropriately evaluate the wind-resistant performance of mechanically attached single-ply membrane roofing systems under dynamic wind loading. In Europe, Gerhardt and Kramer [3], [4] developed a test procedure [5] for fatigue evaluation of roof assemblies based on wind climate data. They mentioned that cracks in the steel deck around the boreholes might occur in areas of high external suction while untwisting of the fixation elements might occur when the metal deck was vibrating under relatively small wind loads. Cook [6] investigated the dynamic response of single-ply membrane roofing systems using the Building Research Establishment's Real-Time Wind Uniform Load Follower (BRERWULF) at Building Research Establishment (BRE), UK; regarding this facility, see Cook et al. [7]. They indicated that static proof testing methods might be inappropriate. In North America, the National Research Council of Canada (NRC) formed an industrial-based consortium called 'Special Interest Group for Dynamic Evaluation of Roofing Systems (SIGDERS)' to develop a test procedure for certifying membrane roofing systems under dynamic wind loading. Wind tunnel investigations were carried out using two flexible roofing membranes, i.e., Polyvinyl Chloride (PVC) and Ethylene Propylene Diene Monomer (EPDM), at full scale. Using the wind tunnel pressure records as source data and comparing the membrane responses of PVC with those of EPDM, SIGDERS developed a dynamic load cycle for mechanically attached membrane roofing systems [8], [9]. Chen et al. [10] and Baskaran et al. [11] evaluated the wind-resistant performance of modified bituminous and thermoplastic roofing systems using three different test methods; i.e., the Factory Manual FM-4470 static test standard [12], the UEAtc procedure and the SIGDERS-developed dynamic load cycle. Comparison of the data obtained from these experiments showed that the static test protocol not only overestimated the design parameters (wind uplift pressure and fastener loads) but also produced fastener pull-out failure mode, whereas the UEAtc and SIGDERS tests produced failure modes similar to those observed in the field. Subsequently, Baskaran and his research group tested various roofing systems using the SIGDERS dynamic wind test protocol at the Dynamic Roofing Facility (DRF) of NRC [13]-[19]. Besides these studies, Silva et al. [20] carried out wind uplift tests on mechanically attached membrane roofing systems according to the guideline for European Technical Approval Guidelines, ETAG 006 [21].

Baskaran and Borujerdi [22] and Baskaran and Molleti [23] developed a finite element model for investigating the impact of table size on the performance of roofing systems under static loading, focusing on the fastener loads.

Comparing the results of extensive numerical simulations with the experimental data, they suggested the required table size and curves for determinations of appropriate correction factors as a function of fastener spacing and fastener row spacing. Further, Baskaran et al. [24] developed a three-dimensional finite element model for predicting membrane deformation, which was validated by a series of benchmark experiments carried out at DRF of NRC. In the numerical and experimental analyses, uniform pressure was applied over the surface of the membrane within the elastic range of material. Prevatt et al. [25] experimentally investigated the effects of specimen sizes on the static wind uplift performance and failure loads of mechanically attached single-ply roofing membranes. The results suggested that correction factors were necessary for comparing tests on different test tables.

Baskaran and Dutt [26] investigated the static and dynamic pull-out strengths of the roof fasteners installed in metal and wooden decks. In the dynamic test, a cyclic horizontal force was applied to the fastener in addition to a vertical pulling force. Based on the results, they suggested that one should use for the fasteners the allowable design load derived from dynamic testing because rotation and rocking of fasteners would occur when the fasteners were exposed to multi-directional wind forces. It was also found that fatigue played an important role in the pull-out resistance of fasteners.

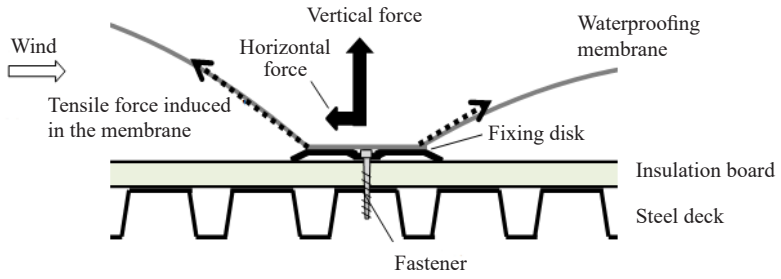


**Figure 2.** Deformation of waterproofing membrane and forces acting on the fastener

All of the above-mentioned studies dealt with the mechanically attached membrane roofing system generally used in Europe and North America. As mentioned above, the roofing system used in Japan is somewhat different from it. Circular steel disks to which the membrane is glued or heat-adhered are mechanically anchored to the structural substrate by fasteners arranged in a square lattice-like form with a spacing of 0.45-1.0 m (typically 0.6 m). Currently, the wind-resistant safety of roofing systems is generally verified by wind resistance tests, as per JASS 8 [27] or by simplified dynamic pressure tests in Japan. Thus, Uematsu et al. [28] proposed a dynamic wind load cycle model for evaluating the wind-resistant performance of a mechanically attached single-ply membrane roofing system focusing on the fatigue damage, based on a wind tunnel experiment conducted by Furuichi et al. [29]. Following significant damage to waterproofing systems caused by strong winds of Typhoon No. 18 of 2004 in Japan, Miyauchi et al. [30], [31] carried out extensive research on the wind-induced behavior and wind-resistant performance of mechanically attached single-ply membrane roofing systems. First, they carried out a field measurement of wind pressures and wind-induced responses (membrane deformations and fastener loads) of a roofing system installed on a full-scale flat-roofed test building without parapets, 6 m long, 6 m wide, and 3 m high, during a typhoon. They found that the fasteners located near the windward roof corner were subjected to horizontal forces as large as vertical ones. Then, they carried out a pressure test and a wind tunnel test using a full-scale roofing assembly. In the pressure test, the membrane was subjected to uniform pressure on the bottom surface, which is equivalent to uniform suction on the top surface. Therefore, no lateral force was generated on the fasteners. On the other hand, in the wind tunnel test, the test model was immersed in a turbulent boundary layer, and therefore the wind pressures (suctions) on the roof varied in the windward direction. Accordingly, the membrane deflection varied in the wind direction too, resulting in lateral forces at the fixing points, as shown in Figure 2. Note that the wind tunnel experiment did not reproduce wind pressure distributions on any practical roofing system, because the geometric similarity was not satisfied. They proposed an empirical formula for predicting the lateral forces based on the difference between wind pressure coefficients on the windward and leeward sides of the fastener. The application of this formula is questionable because the mechanical properties of the membrane are not

considered in the formula, even though the horizontal force is related to the membrane deformation (Figure 2). Tanaka et al. [32], [33] developed simple test methods for evaluating the wind-resistant performance of mechanically attached waterproofing membranes considering the effect of horizontal forces.

The lateral forces may affect the pull-out strength of fasteners significantly, particularly for steel decks. Therefore, for evaluating the wind-resistant performance of roofing systems it seems important to understand the fundamental characteristics of the wind forces acting on the fasteners not only in the vertical direction but also in the horizontal direction. In the present study, we have developed a test method using three Pressure Loading Actuators (PLAs) for investigating this subject [34]. Two series of experiments on full-scale roofing assemblies are carried out using this facility. The fluctuating pressures applied to the specimen are generated by using the time history of wind pressure coefficients at three points near the windward roof corner obtained from a wind tunnel experiment. Furthermore, we have developed a finite element model of the roofing system, which is verified by an experiment with a full-scale specimen. Finally, we analyze the dynamic responses of a practical roofing system using this finite element model.

It should be noted that the present paper focuses mainly on the stationary behavior of the roofing system in synoptic winds. Non-stationary phenomena such as tornadoes and down-bursts are out of the scope of this study.

## 2. Investigated building and roofing assembly

The subject of the present study is a mechanically attached single-ply membrane roofing system installed on flat roofs of middle-rise and high-rise buildings with or without parapets (see Figure 3). The breadth $B$, depth $D$, and height $H$ are respectively 18 m, 9 m, and 18 m for the middle-rise building, and 30 m, 10 m, and 30 m for the high-rise building. The height and thickness of parapets are 0.5 m and 0.2 m, respectively.

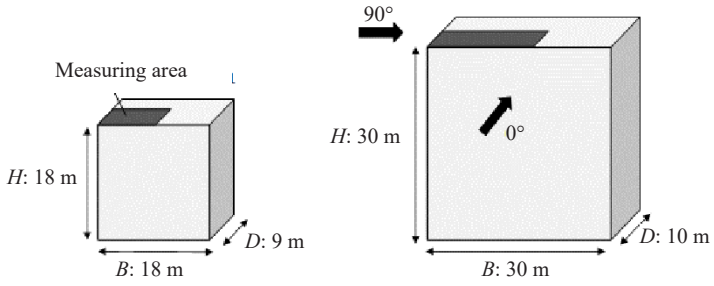


(a) Middle-rise building (b) High-rise building

**Figure 3.** Model buildings and definition of wind direction

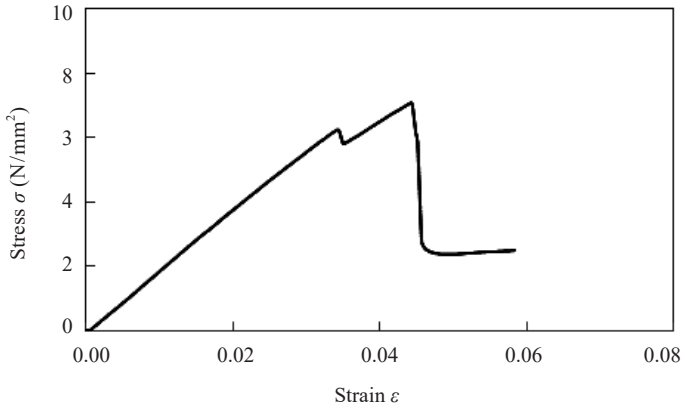


**Figure 4.** Stress-strain relationship of the waterproofing membrane

The waterproofing membrane is Polyvinyl Chloride (PVC) resin sheet of 1.5 mm thickness, reinforced by glass fiber of 33.7 dtex with a density of 4 fibers per 10 mm in both longitudinal and transverse directions. The mass per unit area is 2.1 kg/m$^2$. Figure 4 shows the stress-strain ($\sigma$-$\varepsilon$) relationship of the membrane obtained from a tensile test using a No. 2 dumbbell-type specimen. The relationship is almost linear up to a strain of $\varepsilon \approx 3.5\%$. The tensile strength rapidly changes at $\varepsilon \approx 4.5\%$ due to the fracture of glass fibers. The membrane is placed on a 50 mm thick insulation board of rigid urethane foam and mechanically anchored to a 1.0 mm thick galvanized steel deck (profile height: 75 mm, flute width: 200 mm) by using circular steel disks (diameter: 89 mm, thickness: 0.6 mm) and screws (length: 75 mm, outer diameter: 5.7 mm, inner diameter: 3.7 mm, pitch: 1.8 mm). The disks are arranged in a square lattice-like form with a spacing of 0.6 m, to which the membrane is heat-adhered.

# 3. Wind tunnel experiment of wind pressure distributions on flat roofs

## 3.1 *Experimental apparatus and procedure*

In the wind tunnel experiment, we measure the wind pressure distributions on the roofs. Wind pressures on flat roofs have been studied extensively by many researchers [1], [35]-[39]. The objective of the present experiment is not to investigate the characteristics of wind pressures on flat roofs in detail but to find the most critical condition (wind direction and roof area) for discussing the wind-resistant performance of the roofing system. The time history of wind pressure coefficients at many points under such a condition will be used for the dynamic loading test with a full-scale specimen in Section 4 as well as for the finite element analysis of wind-induced responses of the roofing system in Section 5.

The geometric scale ($\lambda_L$) of the wind tunnel model is assumed 1/100 for the middle-rise building and 1/150 for the high-rise building considering the dimensions of the building model and wind tunnel. As mentioned above, the membrane is anchored to the structural substrate (steel deck) by fasteners arranged in a square lattice-like form with a spacing of 0.6 m. Pressure taps of 0.5 mm diameter are drilled at the center of the lattice in the windward quarter area of the roof (shaded area in Figure 3). The wind direction $\theta$, defined as shown in Figure 3, is changed from 0° to 90° at an increment of 5°.

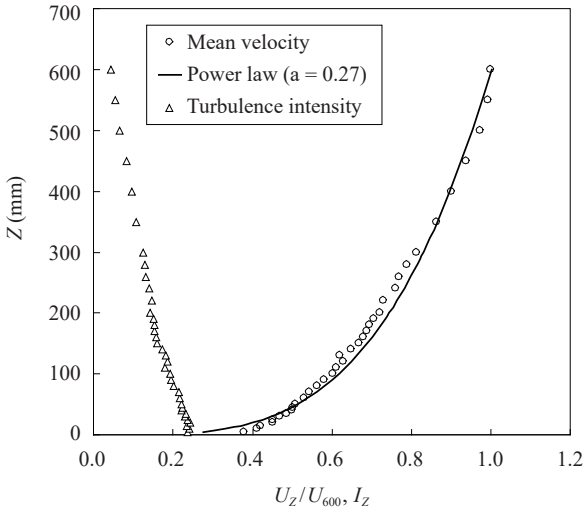


**Figure 5.** Profile of wind tunnel flow

The wind tunnel experiment is carried out in an Eiffel-type wind tunnel at the Department of Architecture and Building Science, Tohoku University, the working section of which is 1.4 m wide, 1.0 m high, and 6.5 m long. The wind tunnel flow is a turbulent boundary layer generated by a standard spire-roughness technique. Figure 5 shows the profiles

of mean wind velocity and turbulence intensity of this flow at the location of the model center without a model. In the figure, $U_{600}$ represents the mean wind velocity at a reference height of $Z$ = 600 mm. The power-law exponent $\alpha$ of the mean wind velocity profile is approximately 0.27. The turbulence intensity $I_H$ at the model height $H$ is approximately 0.15. Figure 6 shows the power spectrum of wind velocity fluctuations in the longitudinal direction at a height of 0.1 m, which corresponds well to the Karman-type spectrum with an integral length scale $L_x$ of approximately 0.2 m. The present study does not address specific buildings in a specific area. However, compared with the values specified in the Recommendations for Loads on Buildings [40] for Terrain Category III (suburban exposure), the value of $\alpha$ is somewhat large, while the values of $I_H$ and $L_x$ are small. Such discrepancies can be accepted because the main purpose of the present study is to investigate the fundamental characteristics of wind-induced responses of mechanically attached single-ply membrane roofing systems.

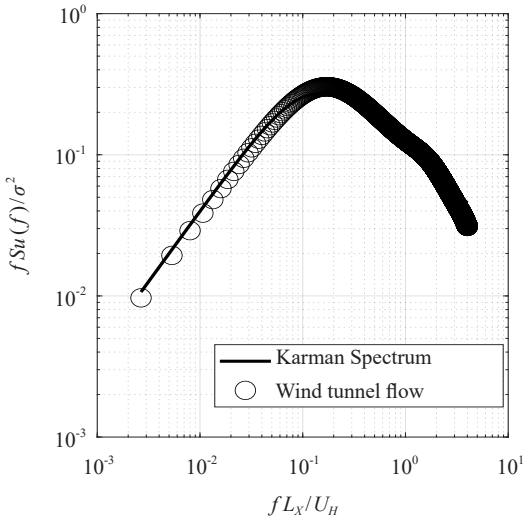


**Figure 6.** Power spectrum of wind velocity fluctuation compared with the Karman-type model

The design wind speed $U_H$ at the roof height $H$ is determined based on the AIJ Recommendations for Loads on Buildings [40], assuming that the '*Basic wind speed*' $U_0$ is 35 m/s and the terrain category is III. In practice, the value of $U_H$ is calculated as 31.3 m/s for the middle-rise building and 34.6 m/s for the high-rise building. In the wind tunnel experiment, $U_H$ is set to 9 m/s for both models; the corresponding Reynolds number defined by $Re = U_H \cdot H/\nu$, with $\nu$ being the coefficient of kinematic viscosity of air is approximately $1.1 \times 10^5$ for the middle-rise building and approximately $1.2 \times 10^5$ for the high-rise building. The blockage ratio determined based on working section dimensions of the boundary layer wind tunnel is approximately 2.6% and 3.0% for the middle-rise and high-rise building models, respectively. The Reynolds number and the blockage ratio of the wind tunnel experiment satisfy the experimental criteria recommended by the Wind Tunnel Testing for Buildings and Other Structures [41]. Thus, the minimum model Reynolds number is larger than $1.1 \times 10^4$ and the maximum wind tunnel blockage radio is smaller than 5%. The velocity and time scales, $\lambda_V$ and $\lambda_T$, of the wind tunnel experiment are respectively 1/3.48 and 1/28.8 for the middle-rise building and 1/3.84 and 1/39.0 for the high-rise building. Wind pressures at all pressure taps are sampled simultaneously at a rate of 800 Hz for a time duration of 10 min at full scale using a multi-channel pressure measuring system (Wind Engineering Institute, MAPS-02). A low-pass filter with a cut-off frequency of 300 Hz is used to remove high-frequency noises from the signals. The distortion of the measured wind pressures is compensated by using the frequency response function of the measuring system in the frequency domain. The measurements are repeated 10 times under the same condition. The wind pressure is converted to a pressure coefficient $C_p$ defined in terms of the velocity pressure $q_H$ of the approach flow at the roof height $H$. The statistical values of $C_p$ are obtained by applying the ensemble average to the results of the consecutive 10 runs.

### 3.2 *Experimental results*

It is well accepted that large suctions are induced near the windward corner of a flat roof in an oblique wind due to the generation of conical vortices (see [1], for example). In the high-suction zone, the pressure gradient is also large. As a result, large vertical and horizontal forces may be generated on the fasteners, as mentioned above (see Figure 2). Thus, the condition (pressure tap and wind direction) generating the most critical negative peak pressure coefficient, $C_{p,\mathrm{cr}}$, irrespective of wind direction and pressure tap location was first detected. The wind direction providing $C_{p,\mathrm{cr}}$ was found to be 35° for the middle-rise building and 40° for the high-rise building. Figure 7 shows the distribution of the minimum peak pressure coefficients on each roof at such a wind direction. Note that the values in each sub-figure do not necessarily occur at the same time. The location of pressure taps is represented by '+' in the figure. The largest peak suction occurs at a windward pressure tap located near the windward corner. Then, three pressure taps including this one are selected to obtain the time history of wind pressure coefficients to be used for the dynamic response test on a full-scale specimen in the next section. The selected pressure taps are located in a rectangle shown in each sub-figure of Figure 7; the wind pressures at these pressure taps are called Loads A to C in order from the edge. It is also found from Figure 7 that the parapets reduce the magnitude of $C_{p,\mathrm{cr}}$ significantly and flatten the distribution of negative peak pressure coefficients. The effects of parapets on the pressure distributions on flat roofs have been investigated by many researchers[29], [35], [42]-[50]. The present results are consistent with the results of these previous studies.

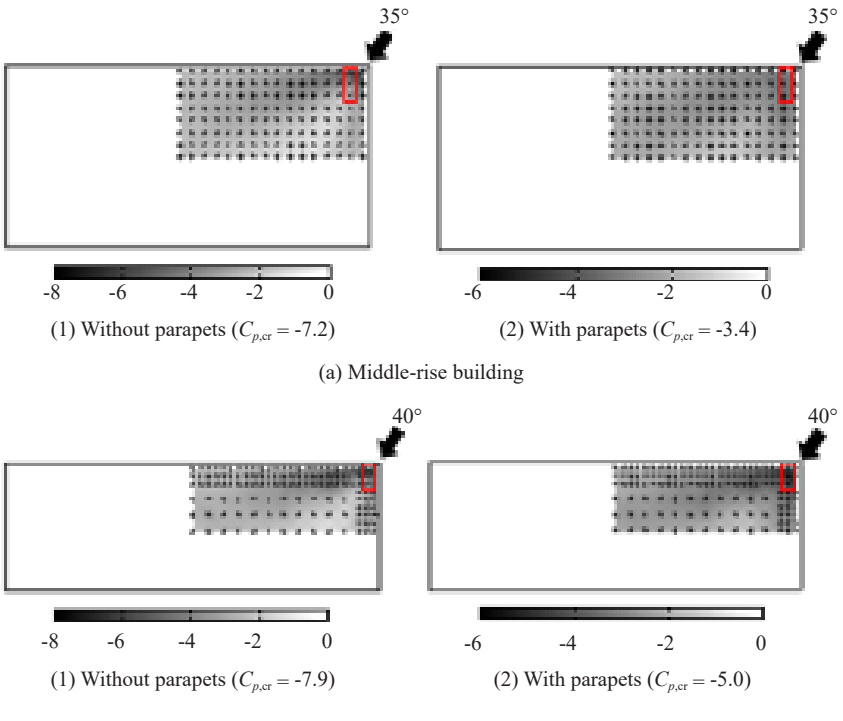


**Figure 7.** Distribution of the minimum peak pressure coefficients together with the pressure tap arrangement

## 4. Experimental program for evaluating the wind-resistant performance of roofing system

### 4.1 *Objectives and experimental facility*

Two series of experiments are conducted in the present study. The objective of the first series of experiments is to investigate the dynamic response of the mechanically attached single-ply membrane roofing system under practical

conditions, while that of the second series of experiments is to investigate the failure mode and load under final conditions.

We have developed an experimental facility for evaluating the wind-resistant performance of full-scale specimens of cladding, which consists of three Pressure Loading Actuators (PLAs) and a chamber to which a test specimen is attached (see Figure 8). The size of the chamber is 2.0 m × 2.2 m in plan and 0.2 m in depth. The PLA was originally developed by Kopp et al. [51] at The University of Western Ontario, Canada. It can generate the fluctuating pressures on the roof of a practical building almost faithfully using the time history of wind pressure coefficients obtained from a wind tunnel experiment. In practice, the facility could reproduce fluctuating wind pressures up to approximately 4 Hz at the maximum pressure level of 3-4 kPa almost faithfully. The root coherence between the target signal and the output was approximately 0.9 at a frequency of 4 Hz. Furthermore, the PLA can reproduce the designated pressure fluctuations faithfully through a feedback control even when the membrane deformation becomes large enough to affect the cavity pressure or when a small amount of air leakage occurs due to the tear of the membrane. Regarding the details of this facility, see Gavanski et al. [52]. This facility has been used for studying the wind-resistant performance of various cladding systems [53], [54].

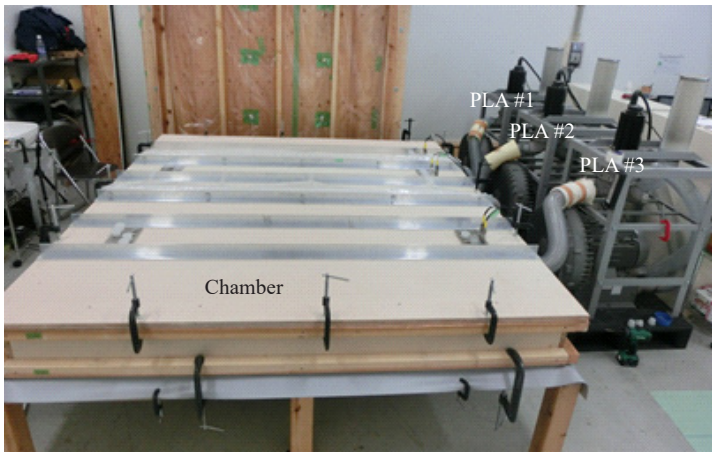


**Figure 8.** Dynamic roofing facility

## 4.2 *Experimental setup*

The experimental setup for the first series of experiments is schematically illustrated in Figure 9. The specimen represents a part of a full-scale mechanically attached single-ply membrane roofing system located near the roof corner. The membrane is clamped along the chamber walls and mechanically anchored to the baseplate of the chamber by steel disks and fasteners at nine locations arranged in a square lattice-like form with a spacing of 0.6 m. Because the purpose of this series of experiments is to measure the membrane deformation and the wind forces acting on the fasteners, a 24-mm thick plywood is used for the baseplate (structural substrate); that is, neither the insulation board nor the steel deck is used. The chamber is divided into three spaces, called Spaces A to C, by using 0.2 mm thick silicon sheets. It was confirmed that the silicon sheets did not affect the behavior of the waterproofing membrane significantly. Two six-component force balances (KYOWA, LFM-A-3kN) are installed at Points $P_A$ and $P_B$, to which the disks are fixed by bolts. The force balances measure the forces, $F_x$, $F_y$, and $F_z$, in the $x$, $y$, and $z$ directions, acting on the disks. The resonant frequency is 5 kHz and the cut-off frequency of the amplifier is 500 Hz. Five laser displacement meters (KEYENCE, IL-300) are installed at Points LDT1 to LDT5 to measure the membrane deflections at these points. Pressures in Spaces A to C (Loads A to C) are separately controlled by using three PLAs. The pressures in these spaces are measured by three differential pressure transducers (Sensortechnics, CTEM7N350GL0). The pressures in Spaces A to C, the forces $F_x$, $F_y$, and $F_z$ at Points $P_A$ and $P_B$, and the membrane deflections at Points LDT1 to LDT5 are sampled at a rate of 200 Hz simultaneously.

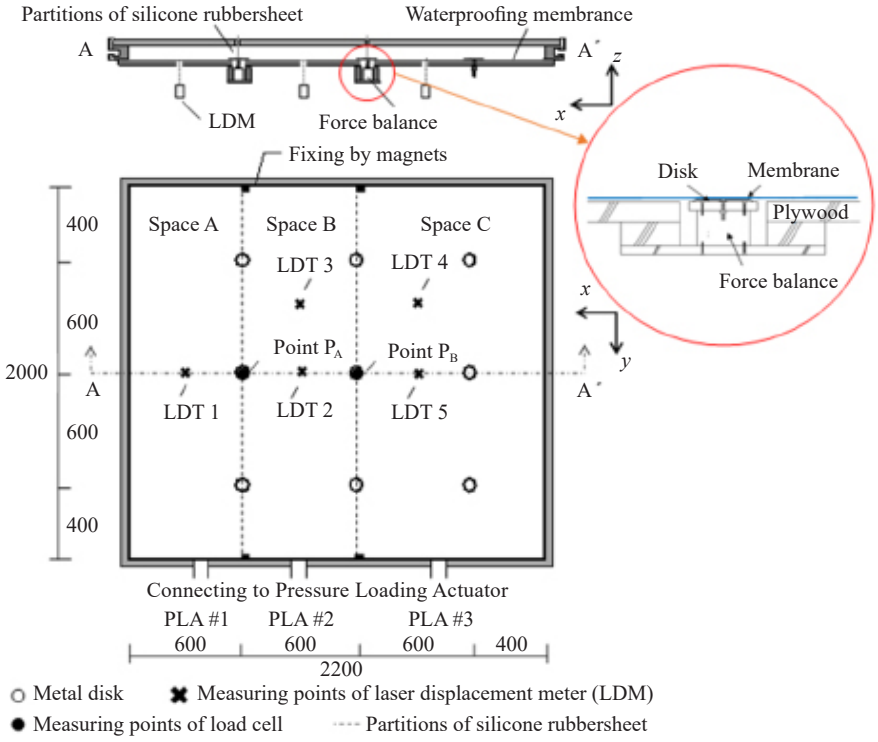


**Figure 9.** Experimental setup; specimen and chamber [unit: mm]

The following three kinds of loading are used in the experiments:

1. Ramp pressure loading (RP): uniform negative pressure decreasing at a rate of 1 kPa/min is applied to the whole space without silicon sheets.

2. Single-space realistic wind loading (SRP): Load A for the middle-rise building without parapets is applied to the whole space without silicon sheets.

3. Three-space realistic wind loading (3RP): Loads A to C are applied to Spaces A to C separately. Figures 10 and 11 respectively show the time history of fluctuating pressures $p(t)$ applied to Spaces A to C (Loads A to C) for the middle-rise and high-rise buildings with or without parapets, where $p(t)$ is given by the following equation:

$$p(t) = \frac{1}{2}\rho U_H{}^2 C_p(t) \tag{1}$$

in which $\rho$ is the air density, $U_H$ is the design wind speed at the roof height $H$, and $C_p(t)$ is the wind pressure coefficient as a function of time $t$. Note that a ramped pressure for a period of 10 s is applied first to avoid unrealistic responses of the membrane to stepwise loading. It is clear that the pressure fluctuations are dependent on the location and affected by the parapets significantly.

In the second series of experiments, the specimen is constructed of practical roofing components. The structural substrate is a steel deck, and an insulation board is inserted between the waterproofing membrane and the steel deck. The loading conditions are the same as those for the first series of experiments. Neither the fastener loads nor the membrane deflections are measured. First, we apply 600-second dynamic pressure to the specimen six times. After that, we observe the state and degree of damage to the roofing assembly. If the specimen is not broken, a ramped pressure decreasing at a rate of 1 kPa/min is further applied to the specimen until it fails. Finally, we observe the failure mode.

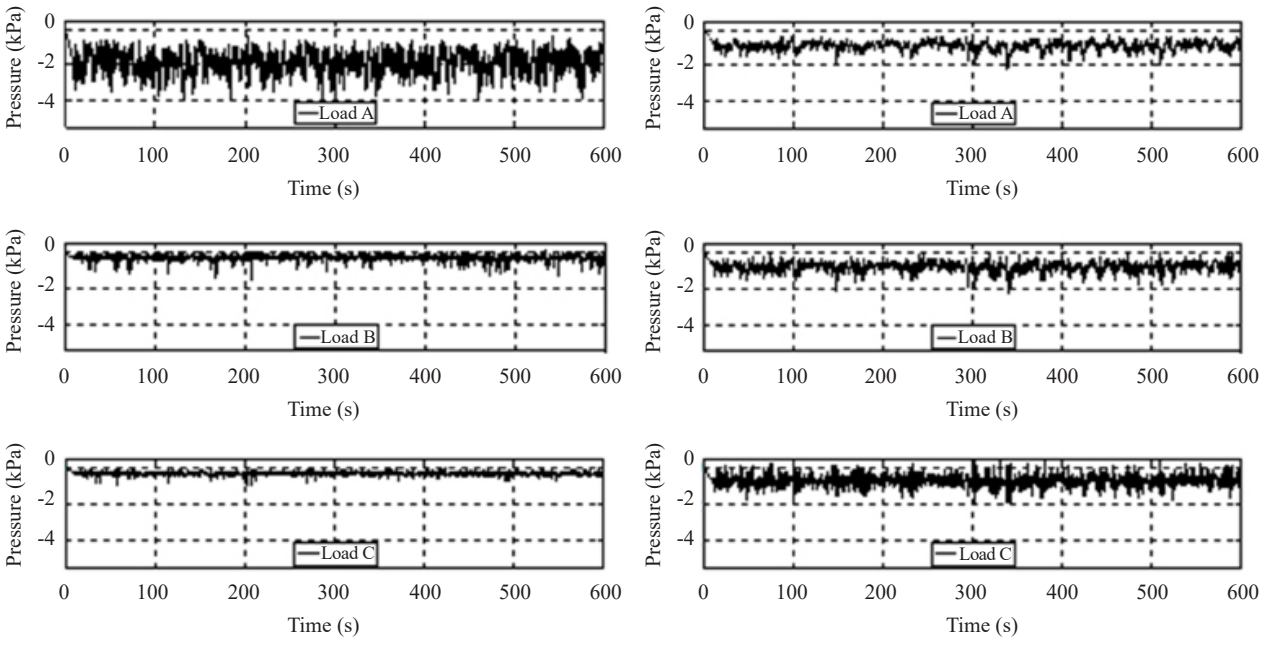


**Figure 10.** Time history of pressures in Spaces A to C (middle-rise building)

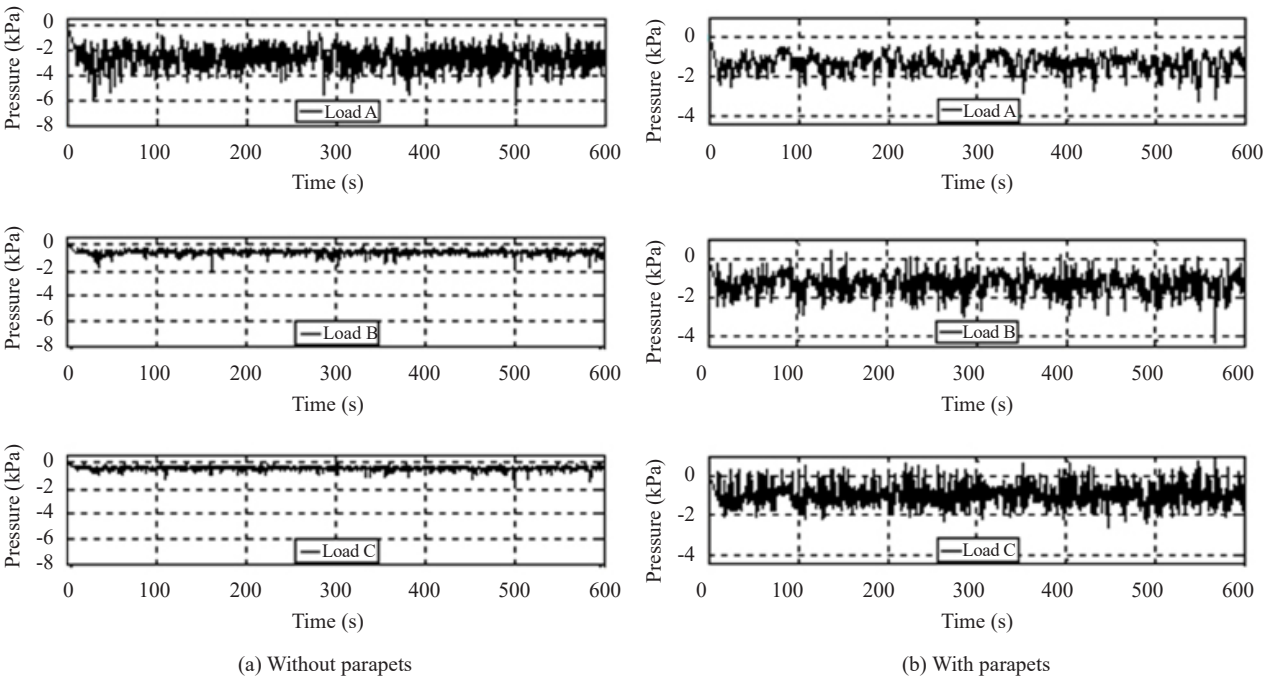


**Figure 11.** Time history of pressures in Spaces A to C (high-rise building)

## 4.3 *Results and discussion*

Figure 12 shows the time history of $F_x$ and $F_z$ measured at Point $P_A$ for the middle-rise building with or without parapets under various loading conditions. Note that $F_y$ is not generated in this experiment, because the pressure acting

on the specimen does not vary in the $y$-direction and, therefore, the membrane deformation is symmetric with respect to the centerline along the $x$-axis. In the cases of *Ramp pressure loading* and *Single-space realistic wind loading*, where the pressure in the chamber fluctuates as a whole, the magnitude of $F_x$ is generally small, as shown in Figures 12(a) and 12(b). In these sub-figures, the value of $F_x$ sometimes changes discontinuously. This phenomenon occurs at a moment when the reinforcing fiber breaks. On the other hand, in the case of *Three-space realistic wind loading*, where the pressure varies with space, the magnitude of $F_x$ becomes rather large, particularly for buildings without parapets, as shown in Figure 12(c). Figure 13 shows the results for the high-rise building with or without parapets in the case of *Three-space realistic wind loading*. Similar to the middle-rise building, large horizontal forces $F_x$ are induced in the case of the building without parapets. Table 1 shows the maximum peak values of $F_x$ and $F_z$ in the *Three-space realistic wind loading* case. It can be seen that horizontal forces nearly equal to or larger than the vertical ones are generally generated on the fasteners. Such an experimental result is consistent with the finding of Miyauchi et al. [30] in the field observation made on a full-scale test building during a typhoon. In the case of buildings with parapets, the mean value of $F_x$ is generally small in magnitude. This feature is related to a fact that the spatial variation of mean wind pressures on the roof is relatively small. However, the fluctuation of $F_x$ is rather large, which may be due to a large spatial variation of instantaneous wind pressures acting on the roof. It is thought that the horizontal forces affect the wind-resistant performance of the roofing systems significantly because an additional moment is generated at the fixing point of the fastener by the horizontal force, which may reduce the fastener's pull-out resistance significantly. Most of the current wind resistance evaluation tests for roofing systems do not consider the effects of such a horizontal force. Therefore, it is hoped to develop a new test method considering the effects of horizontal forces appropriately.

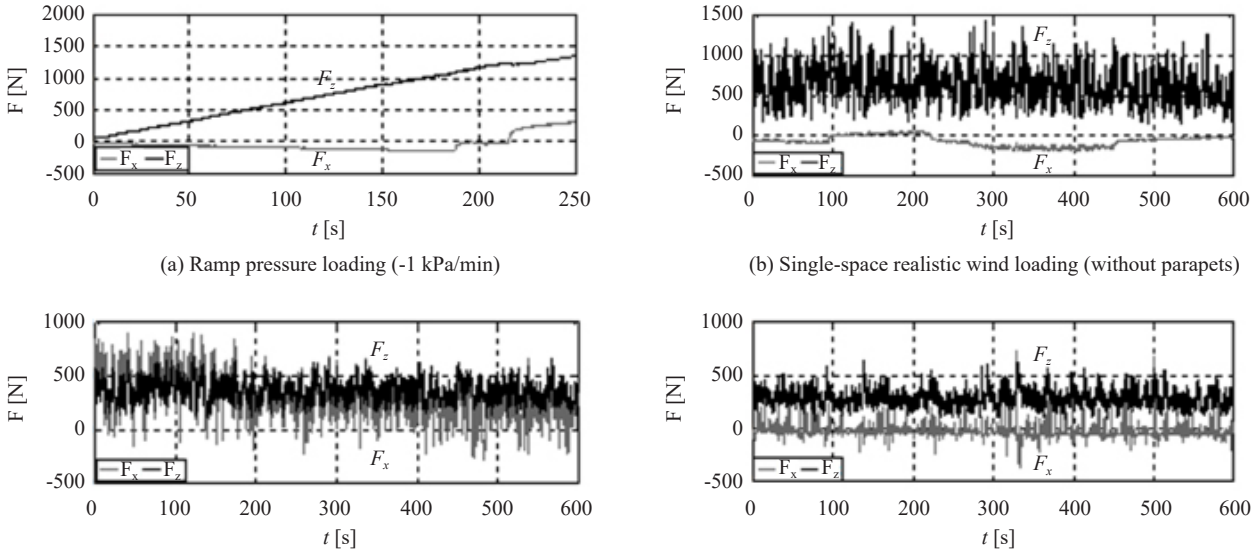


**Figure 12.** Time history of horizontal force $F_x$ and vertical force $F_z$ acting on the fastener at Point $P_A$ (middle-rise building)

Table 2 summarizes the mean deflections of the membrane at Points LDT1 to LDT5. In the SRP case, the largest deflection occurs at Point LDT3. In the 3RP case, on the other hand, the large deflection occurs at LDT1 for buildings without parapets and LDT4 for buildings with parapets. The difference between the deflections at Points LDT1 and LDT2 is large for buildings without parapets; this feature corresponds well to the above-mentioned finding that the mean $F_x$ value at Point $P_A$ is large in such a case. On the other hand, the difference between the deflections at Points LDT1 and LDT2 is relatively small for buildings with parapets, which corresponds well to the fact that the mean $F_x$ value at Point $P_A$ is very small in magnitude. These results indicate that the horizontal forces generated at the fixing points are related to the membrane deformation.

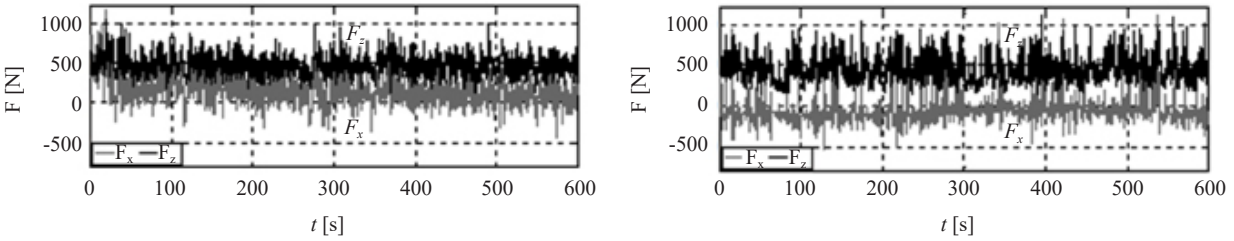


(a) Three-space realistic wind loading (without parapets)

(b) Three-space realistic wind loading (with parapets)

**Figure 13.** Time history of horizontal force $F_x$ and vertical force $F_z$ acting on the fastener at Point $P_A$ (high-rise building)

**Table 1.** Maximum wind forces in the $x$ and $z$ directions (unit: N)

| Building | Parapet | Point $P_A$ | | Point $P_B$ | |
|---|---|---|---|---|---|
| | | $F_{x,\max}$ | $F_{z,\max}$ | $F_{x,\max}$ | $F_{z,\max}$ |
| Middle-rise | without | 906 | 687 | 464 | 376 |
| | with | 731 | 631 | 793 | 708 |
| High-rise | without | 1170 | 1054 | 715 | 525 |
| | with | 1122 | 1110 | 1049 | 991 |

**Table 2.** Mean deflection of the membrane (unit: mm)

| Loading condition | Building | Parapet | LDT1 | LDT2 | LDT3 | LDT4 | LDT5 |
|---|---|---|---|---|---|---|---|
| SRP | Middle-rise | without | 67.7 | 85.7 | 98.7 | 94.9 | 82.0 |
| | | with | 45.0 | 45.7 | 66.3 | 64.9 | 47.1 |
| 3RP | Middle-rise | without | 62.9 | 38.5 | 56.9 | 45.5 | 32.8 |
| | | with | 48.7 | 47.2 | 67.7 | 64.7 | 47.7 |
| | High-rise | without | 81.2 | 41.9 | 61.2 | 56.2 | 41.0 |
| | | with | 60.8 | 70.0 | 89.0 | 76.3 | 55.2 |

SRP: Single-space realistic wind loading, 3RP: Three-space realistic wind loading

Table 3 summarizes the results for the failure loads and modes. Three specimens were tested for each loading condition. The damage by realistic wind loading (SRP and 3RP) depends on the loading condition significantly. In the SPR case, no visible damage was observed after the realistic pressures have been applied to the specimen. In the 3RP case, on the other hand, lifting of disks due to untwisting of fasteners occurred in many cases, as shown in Figure 14(a). Note that the white part in Figure 14(a) is due to the reflection of light on the surface of a silicon sheet. In the table 'small', 'medium' and, 'large' represent the amount of lifting, which is less than about 1 mm for 'small', less than about 10 mm for 'medium', and more than about 10 mm for 'large'. In the cases of 'medium' and 'large', the fasteners can pierce the membrane. Considering that the magnitude of pressures is almost the same both in the SRP and 3RP cases, we can conclude that the untwisting of fasteners seem to occur more easily, which may result in a reduction of the pull-out strength of fasteners when lateral forces act on the fasteners. It is found that the amount of lifting is generally larger for the high-rise building than for the middle-rise building. This is due to larger wind forces acting on the fasteners in the high-rise building case. The failure mode at the final stage was generally torn of the membrane around the disks (see Figure 14(b)). The failure loads seem to be less sensitive to the loading condition. Note that relatively small failure

loads for some specimens were due to poor adhesion between disk and membrane. These results imply that the ultimate strength of the membrane is minutely affected by the horizontal forces. Within the limits of the present experiment, in which fluctuating pressure was applied to the specimen for one hour, the effect of horizontal forces on the failure mode and load was not observed clearly. For investigating the fatigue damage of the steel deck we should have applied the fluctuating pressures to the specimen for a longer time. This is the subject of our future study.

**Table 3.** Results of wind resistant performance tests

| | Loading condition | | Damage by realistic wind loading | Failure load (kPa) by ramp pressure loading |
|---|---|---|---|---|
| RP | | | - | -4.9 |
| | | | | -5.3 |
| | | | | -5.0 |
| SRP | | | No damage | -4.1 |
| | | | | -4.8 |
| | | | | -4.6 |
| 3RP | Middle-rise building | without parapets | No damage | -4.9 |
| | | | | -5.0 |
| | | | | -4.8 |
| | | with parapets | Lifting of disks (small) | -5.2 |
| | | | No damage | -5.0 |
| | | | No damage | -5.5 |
| | High-rise building | without parapets | Lifting of disks (medium) | -4.9 |
| | | | Lifting of disks (large) | -4.9 |
| | | | Lifting of disks (medium) | -5.1 |
| | | with parapets | Lifting of disks (large) | -4.3 |
| | | | Failure by Pulling out of fasteners | - |
| | | | Lifting of disks (large) | -5.1 |

RP: Ramp pressure loading

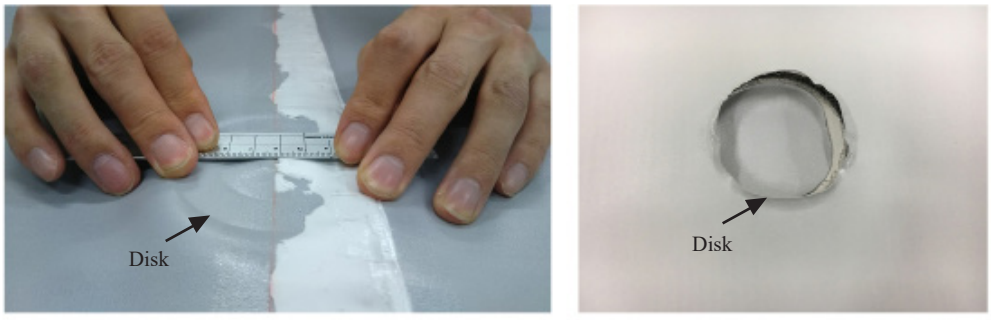


(a) Lifting of disk (Medium) (b) Tear of membrane

**Figure 14.** Damage and failure modes

# 5. Numerical analysis of wind-induced responses of roofing system

## 5.1 *Finite element model*

In the above-mentioned experiment, the size of the specimen is rather limited and the spatial variation of pressures is considered only in the *x*-direction. In contrast, practical roofing systems are much larger in size and the wind pressures vary not only in the *x*-direction but also in the *y*-direction. Therefore, in order to investigate the wind-induced behavior of a practical roofing system, we have developed a 3D finite element model using a commercial software MSC. Marc (Ver. 2014.2) on a supercomputer at Tohoku University Cyber Science Center, in which the geometric nonlinearity is considered, but the fracture of the reinforced fibers is not considered. Because the focus is on the behavior of the membrane and the wind forces acting on the fasteners, the insulation board, the fasteners, and the steel deck are not involved in the model. The membrane deformation due to suctions may affect the wind pressure distribution on the roof due to the Flow-Structure Interaction (FSI), particularly in the case of buildings without parapets. However, this effect is not considered in the present analysis for simplicity. That is, the wind pressures are given by Eq. (1) regardless of the membrane deformation.

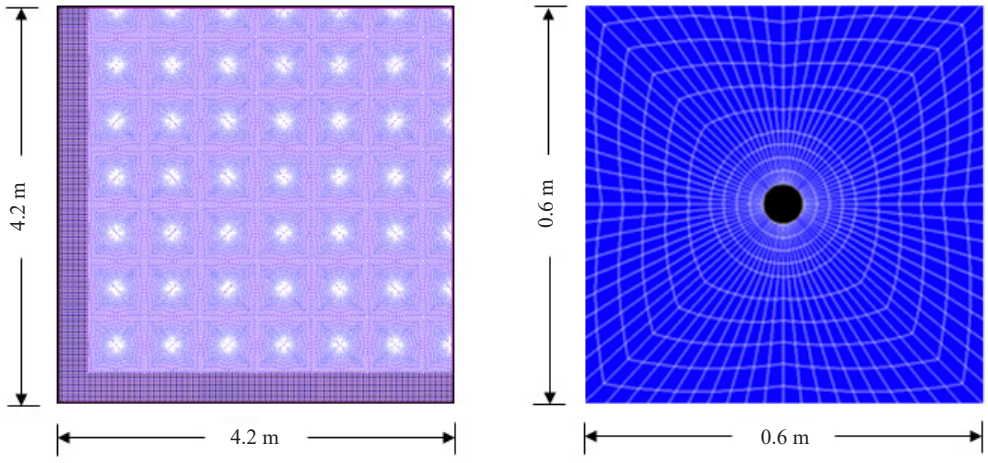


(a) Overall view of analyzed area (b) Local view around a disk

**Figure 15.** Finite element model representing a corner zone (4.2 m × 4.2 m) of the roofing system

Figure 15 shows the finite element model, which represents a part of the waterproofing system near the windward roof corner, 4.2 m by 4.2 m in size; the bottom-left corner of the figure corresponds to the windward roof corner. Figure 15(a) shows the general view of the analyzed area, while Figure 15(b) shows a local view around a disk. The belt-shaped areas along the left and bottom sides and the doughnut-shaped areas around the disks are divided into smaller elements considering the stress concentration. The numbers of elements and nodes are 83,820 and 85,937, respectively. The membrane is clamped to the substrate along the edges. The lower surface of the membrane is fixed to the circular disks of 89 mm diameter arranged in a square lattice-like form with a spacing of 0.6 m. The disks are assumed rigid. The membrane is represented by quadrangular shell elements. The mesh division is determined based on a preliminary analysis focusing on computational accuracy and efficiency. Furthermore, the preliminary analysis indicated that the behavior of the membrane in this area minutely changed even if the analyzed area was expanded.

The membrane is modeled by a composite material consisting of a glass mesh layer and two vinyl chloride layers (sandwich structure). The glass mesh layer is modeled by an anisotropic material of 0.13 mm thickness. The vinyl chloride layer of 0.685 mm thickness is assumed to be a hyperelastic material and modeled by a Mooney-Rivlin model, where the strain energy density function $W$ is represented by the following equation:

$$W = C_{10}(I_1 - 3) + C_{01}(I_2 - 3) \tag{2}$$

where $C_{10}$ and $C_{01}$ are empirically determined material constants, and $I_1$ and $I_2$ are the first and second principal stretches. The total thickness of the sheet is 1.5 mm. The mechanical properties of these materials are summarized in Table 4 and Table 5, which were determined based on the results of uniaxial tension tests made on the membrane. The Newmark's $\beta$ method with $\beta = 1/4$ is employed for solving the equation of motion for the membrane. The structural damping is provided by the Rayleigh type model, assuming that the critical damping ratios of the first and second modes are both 0.1. The wind load applied to each node of the finite element model, acting in the normal direction of the surface, is given by the product of the velocity pressure $q_H$, the wind pressure coefficient $C_p$ and the tributary area $\Delta A$ of the node. The values of $C_p$ at the location of the nodes are obtained from the wind tunnel experiment (Section 3). Because the spatial resolution of pressure taps of the experimental model is much coarser than that of the finite element nodes, the wind pressure coefficients at the nodes are computed by applying the cubic spline function to the experimental data for interpolation and extrapolation. In the dynamic response analyses, the time history of wind pressure coefficients for a period of 600 s including the most critical negative peak pressure coefficient $C_{p,\mathrm{cr}}$ is used. To avoid unrealistic transient responses to stepwise loading a ramped pressure for a period of 10 s is added to the practical one in the same manner as was done in Figures 10 and 11. The time step of computation is 0.04 s. The wind loads at each time step are computed by applying the cubic spline function to the time history of wind pressure coefficients for interpolation.

**Table 4.** Mechanical properties of the materials-Glass mesh layer

| Young's modulus (N/mm$^2$) | | Poison's ratio | Shear modulus (N/mm$^2$) | | | Thickness (mm) |
|---|---|---|---|---|---|---|
| $E_1$ | $E_2$ | $v_{12}$ | $G_{12}$ | $G_{23}$ | $G_{31}$ | |
| 160 | 160 | 0.21 | 0.001 | 930 | 930 | 0.13 |

**Table 5.** Mechanical properties of the materials-Vinyl chloride layer

| Mooney-Rivlin model material constants | | Thickness (mm) |
|---|---|---|
| $C_{10}$ | $C_{01}$ | |
| 0 | 5.312 | 0.685 |

The details of the present finite element analysis, i.e., constitutive law and modeling of the materials, mesh division, boundary condition, and solution of the equation of motion, are described in Sugiyama [55].

## 5.2 *Verification of the numerical model and method*

To investigate the validity of the proposed numerical model and method we computed the responses of a full-scale specimen mentioned in Section 4 and compared the results with the experimental ones. Figure 16 shows the finite element model that simulates the test specimen used in Section 4. The mesh division is similar to that of Figure 15. The numbers of elements and nodes are 19,206 and 18,712, respectively. The time history of pressures applied to Spaces A to C is shown in Figure 17, which is different from that used in Section 4. The time history of wind pressure coefficients used here was obtained from a wind tunnel experiment on a low-rise flat-roofed building, which was carried out as a preliminary study for investigating the finite element model and method to be used for field measurement and the time history was obtained from a wind tunnel experiment at a wind direction of $\theta = 30°$. Because the focus is on the responses in the elastic range of the membrane, the magnitude of applied pressures is smaller than that of Figures 10 and 11. Regarding the details of the experiment, see Sugiyama et al. [34].

Shown in Figure 18 is a schematic illustration of the time-averaged deformation of the membrane, which is consistent with the results of Table 2 in a qualitative sense. Table 6 shows a comparison between experiment and computation for the deflections of the membrane at five locations, Points LDT1-LDT5. It is found that the computed

results are somewhat larger than the experimental ones. This difference may be due to the modeling of the reinforcing fibers. However, the present analysis captures the general behavior of the membrane relatively well.

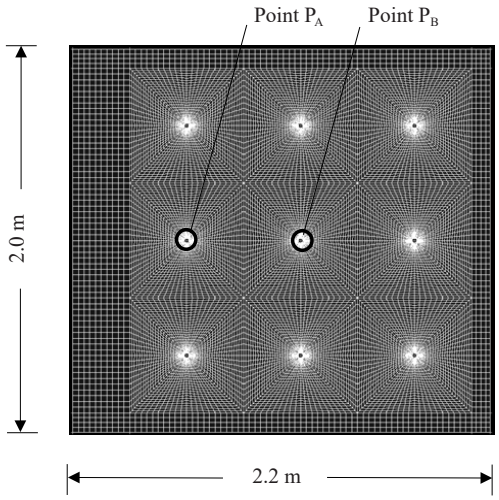


**Figure 16.** Finite element model for validating the computational method

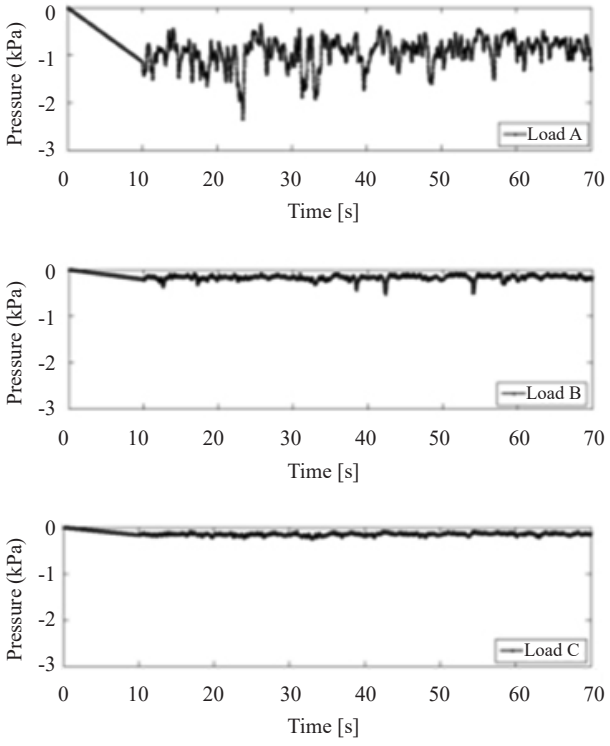


**Figure 17.** Pressure loading for validating the computational method

Figure 19 shows the trajectory of the $F_z$-$F_x$ relationship at Points $P_A$ and $P_B$. The computed results are consistent with the experimental ones not only qualitatively but also quantitatively. It is found that $F_x$ is larger in magnitude than $F_z$. It is interesting to note that the maximum values of $F_x$ and $F_z$ occur almost simultaneously. These results indicate that

the horizontal forces at the fixing points are caused by the non-uniform distribution of wind pressures or the asymmetric deformation of the membrane.

The above-mentioned results imply that the proposed finite element model can reproduce the dynamic response of the roofing system reasonably.

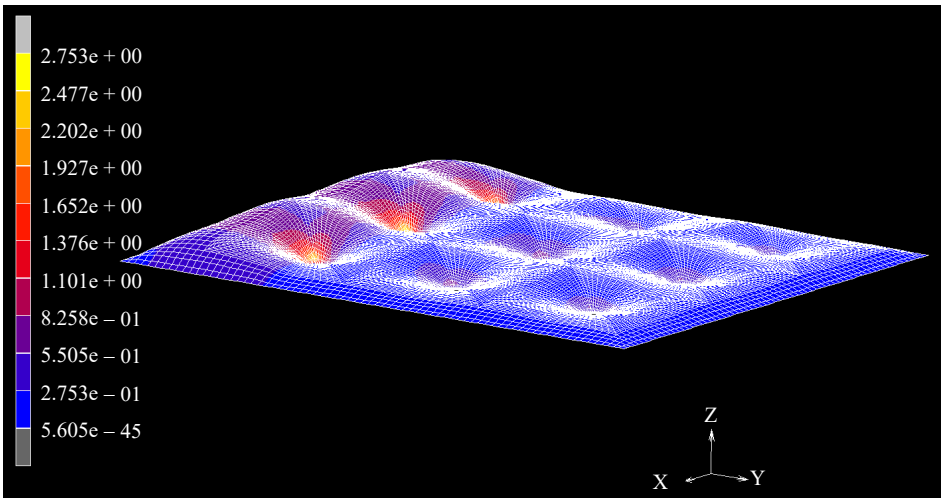


**Figure 18.** Deformation of the waterproofing sheet

**Table 6.** Comparison between experiment and computation for the deflections of the membrane

| Location | Experiment (mm) | | | Computation (mm) | | |
|---|---|---|---|---|---|---|
| | Maximum | Mean | σ* | Maximum | Mean | σ* |
| LDT1 | 48.4 | 38.2 | 2.6 | 58.9 | 43.1 | 4.3 |
| LDT2 | 27.0 | 17.7 | 1.7 | 35.2 | 23.5 | 2.2 |
| LDT3 | 41.4 | 29.0 | 2.1 | 47.6 | 31.8 | 3.0 |
| LDT4 | 28.2 | 24.4 | 1.3 | 35.8 | 31.1 | 1.5 |
| LDT5 | 19.9 | 17.0 | 1.0 | 26.7 | 23.2 | 1.2 |

*σ: standard deviation

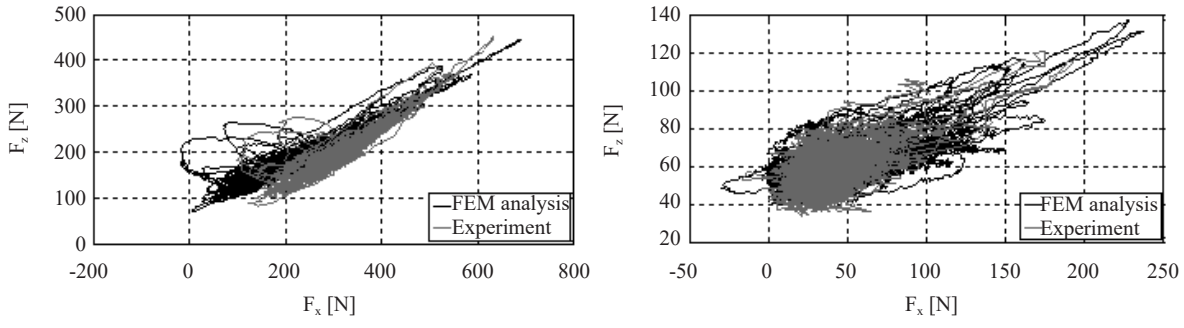


(a) Point $P_A$ (b) Point $P_B$

**Figure 19.** Trajectory of $F_z$-$F_x$ relationship

## 5.3 *Results for the practical waterproofing system*

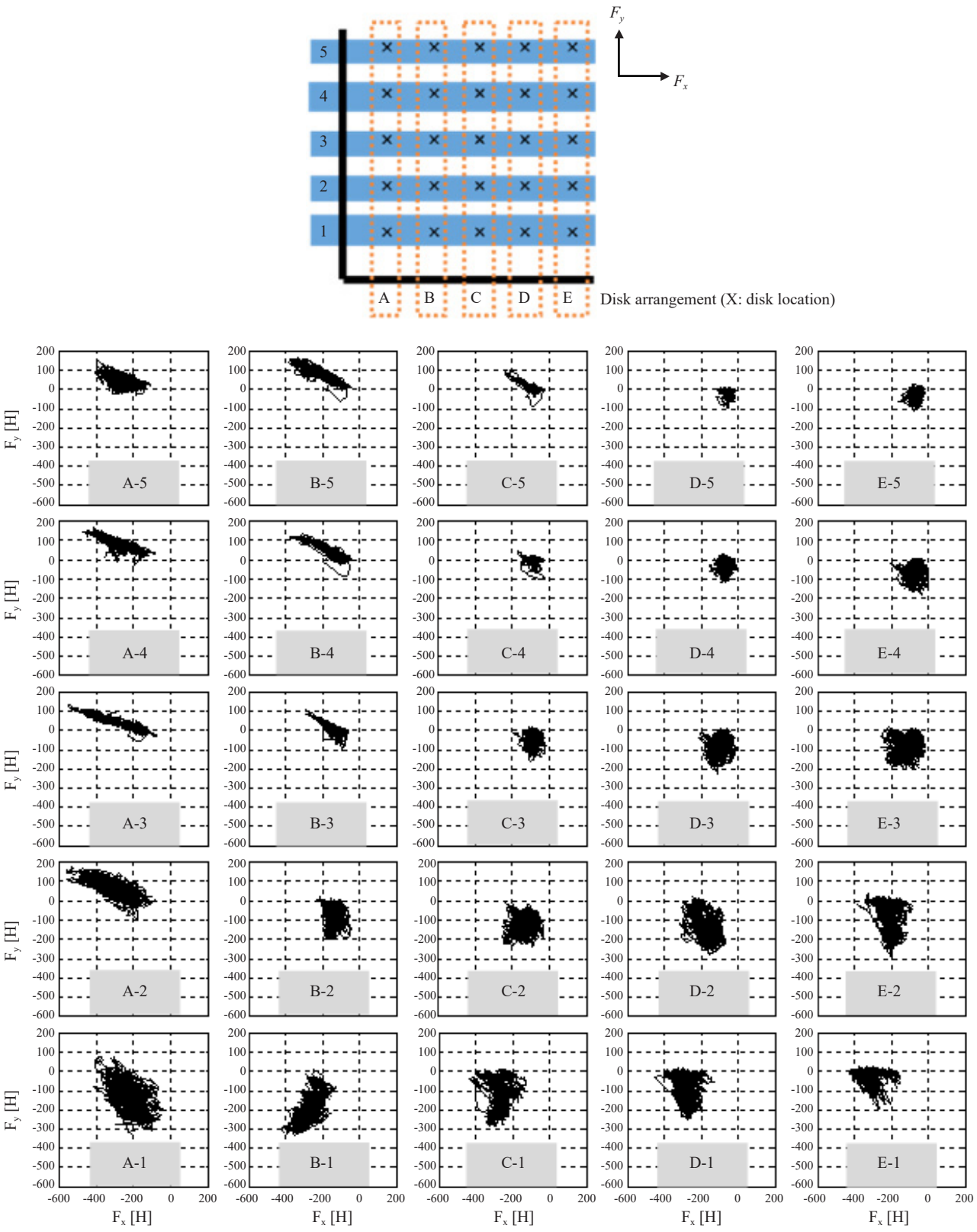


**Figure 20.** Trajectory of $F_y$-$F_x$ relation at 5 × 5 locations of disks (middle-rise building without parapets)

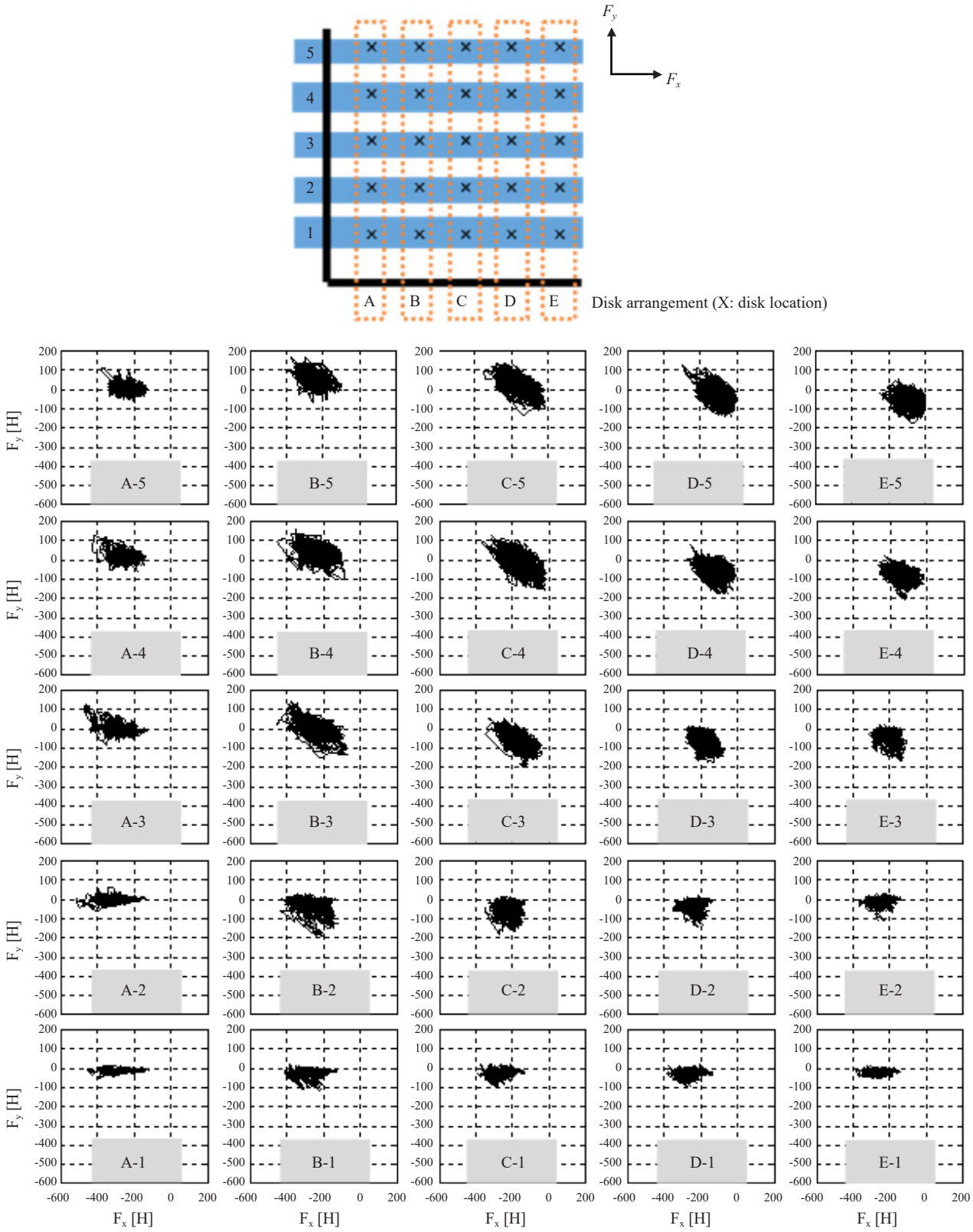


**Figure 21.** Trajectory of $F_y$-$F_x$ relation at 5 × 5 locations of disks (middle-rise building without parapets)

In this section, the wind-induced behavior of a full-scale model shown in Figure 15 is analyzed. Focus is on the horizontal forces at the fixing points. The experiment in Section 4 reproduces horizontal forces only in the *x*-direction. By comparison, the finite element analysis can consider the spatial variation of wind pressures not only in the *x*-direction but also in the *y*-direction, generating horizontal forces in both directions.

Figure 20 shows the trajectories of the $F_y$-$F_x$ relationship at 5 × 5 locations of disks (fasteners) for the middle-rise building without parapets. The vertical and horizontal axes of each subfigure represent $F_y$ and $F_x$, respectively. The location of the disk is represented by '×' and labeled in a matrix form, such as 'A-1', for example. The wind direction is $\theta = 35°$. It is clear that large horizontal forces in the *x* and/or *y* directions are generated on the fasteners located near the roof edge. This feature indicates that the fasteners are subjected to large horizontal forces as well as large vertical forces in this region. In the field region of the roof, on the other hand, the magnitude of $F_x$ and $F_y$ is relatively small, where the fasteners are mainly subjected to vertical forces. The results for the middle-rise building with parapets are shown in Figure 21. It is interesting to note that horizontal forces are relatively large in the field region of the roof, whereas they are relatively small near the edges, compared with no parapet case. The difference in the characteristics of horizontal forces between the buildings with and without parapets may be related to the difference in the membrane deformation.

## 6. Concluding remarks

The present paper investigates the wind-induced dynamic responses of mechanically attached single-ply membrane roofing systems under practical loading conditions, in which the variations of wind pressures acting on the membrane in both time and space are considered.

First, the wind pressures acting on the roofs of middle-rise and high-rise buildings with or without parapets were measured in a turbulent boundary layer. The results indicated that very large peak suctions were induced near the windward corner of the roof in oblique winds. The pressure gradient was also large in such a high suction area.

Then, we have developed a test method for evaluating the wind-resistant performance of the roofing system using three Pressure Loading Actuators (PLAs). The chamber was divided into three spaces by using thin silicon sheets. The PLAs generated different fluctuating pressures in these spaces based on the time history of wind pressure coefficients measured at three different points on the roof near the windward corner in an oblique wind. The deformation of the membrane and the wind forces acting on the fasteners connecting the membrane with the roof deck were measured using a full-scale specimen. The results indicated that horizontal forces nearly equal to or larger than the vertical ones were generated on the fasteners.

Subsequently, the failure loads and modes under various loading conditions were measured using a full-scale assembly of the roofing system. When the fasteners were subjected to ramp pressure loading, the pull-out of fasteners from the steel deck was difficult to occur. The failure mode was a 'tear' of the membrane around the disks. On the other hand, when the fasteners were subjected to high-frequency fluctuating loads in the vertical and/or horizontal directions, lifting of disks due to untwisting of fasteners occurred easily. It was thought that fluctuating wind loads in the horizontal direction might reduce the pull-out resistance of fasteners from the steel deck due to fatigue. However, within the limits of the present experiments, in which fluctuating wind pressures were applied to the specimen for one hour, the effects of horizontal forces on the failure mode and load were not clear. To investigate the fatigue behavior of the fixation we should apply fluctuating pressures to the specimen for a longer period.

Finally, a three-dimensional non-linear finite element analysis was carried out to understand the general behaviour of practical waterproofing systems under realistic wind loading. The method of analysis was first verified by comparing the results with those obtained from the experiment for the membrane deflections and the fastener loads. The results for a larger roof area indicated that large horizontal forces in the *x* and *y* directions were generated on the fasteners. The parapet changed the characteristics of fluctuating wind pressures on the roof significantly, resulting in a significant change in the fastener loads. In the case of buildings without parapets, large horizontal forces were generated on the fasteners located in the edge and corner zones. On the other hand, in the case of buildings with parapets, relatively large horizontal forces were generated on the fasteners located in the field region of the roof.

It can be concluded from these results that the effects of horizontal forces acting on the fasteners should be considered appropriately for evaluating the wind-resistance performance of mechanically attached single-ply membrane

roofing systems. In the current wind resistance evaluation tests generally used in the world, only vertical load, be it static or dynamic, is applied to the specimen. It is hoped to develop a simple testing method considering the effects of horizontal forces appropriately.

In the present study, the wind pressures obtained from a wind tunnel experiment using a rigid model are used in the experiment (Section 4) as well as in the numerical analysis (Section 5). However, the membrane deformation may affect the wind pressures on the membrane due to the Flow-Structure Interaction (FSI), particularly when the parapets are not installed. This FSI effect is not considered in the present study for simplicity. This is the subject of our future study.

## Conflict of interest

The authors declare no conflict of interest.

## References


[1] H. Kawai, "Local peak pressure and conical vortex on building," *Journal of Wind Engineering and Industrial Aerodynamics*, vol. 90, pp. 251-263, 2002.

[2] Architectural Institute of Japan, *Wind damage in 2004 and Lessons*. 2006. (in Japanese)

[3] H. J. Gerhardt and C. Kramer, "Wind induced loading cycle and fatigue testing of lightweight roofing fixations," *Journal of Wind Engineering and Industrial Aerodynamics*, vol. 23, pp. 237-247, 1986.

[4] H. J. Gerhardt and C. Kramer, "Wind loading and fatigue behavior of fixings and bondings of roof coverings," *Journal of Wind Engineering and Industrial Aerodynamics*, vol. 29, pp. 109-118, 1988.

[5] European Union of Agreement, *UEAtc Supplementary guide for the assessment of mechanically fastened roof waterproofing*. M.O.A.T. No. 55-1991, UK member of the UEAtc, British Board of Agreement, PO Box 195, Buchnaills Lane, Warford WD2 7NG, United Kingdom, 1991.

[6] N. J. Cook, "Dynamic response of single-ply membrane roofing systems," *Journal of Wind Engineering and Industrial Aerodynamics*, vol. 41-44, pp. 1525-1536, 1992.

[7] N. J. Cook, A. P. Keevil, and R. K. Stobart, "BRERWULF-the Big Bad Wolf," *Journal of Wind Engineering and Industrial Aerodynamics*, vol. 29, pp. 99-107, 1988.

[8] A. Baskaran and Y. Chen, "Wind load cycle development for evaluating mechanically attached single-ply roof," *Journal of Wind Engineering and Industrial Aerodynamics*, vol. 77 & 78, pp. 83-96, 1998.

[9] A. Baskaran, Y. Chen, and U. Vilaipornsawai, "A new dynamic wind load cycle to evaluate mechanically attached flexible membrane roofs," *Journal of Testing and Evaluation*, vol. 27, no. 4, pp. 249-265, 1999.

[10] Y. Chen, A. Baskaran, and W. Lei, "Wind load resistance of modified bituminous roofing systems," *Construction and Building Materials*, vol. 12, pp. 471-480, 1998.

[11] A. Baskaran, W. Lee, and C. Richardson, "Dynamic evaluation of thermoplastic roofing system for wind performance," *Journal of Architectural Engineering*, vol. 5, no. 1, pp. 16-24, 1999.

[12] Factory Manual Research, *Approval standard: class I roof covers* (4470). Norwood, Massachusetts, USA, 1986.

[13] A. Baskaran, H. Ham, and W. Lei, "New design procedure for wind uplift resistance of architectural metal roofing systems," *Journal of Architectural Engineering*, vol. 12, no. 4, pp. 168-177, 2006.

[14] B. A. Baskaran and S. K. P. Ko, "Optimizing the wind uplift resistance of mechanically attached roof systems," *Journal of Architectural Engineering*, vol. 14, no. 3, pp. 65-75, 2008.

[15] A. Baskaran, S. Molleti, and M. Sexton, "Wind performance evaluation of fully bonded roofing assemblies," *Construction and Building Materials*, vol. 22, no. 3, pp. 343-363, 2008.

[16] S. Molleti, A. Baskaran, and S. K. P. Ko, "Development of a new test method for air intrusion quantification of roofing assemblies," *Journal of Testing and Evaluation*, vol. 36, no. 3, pp. 230-241, 2008.

[17] A. Baskaran and S. Molleti, "Impact of air intrusion on the wind uplift performance of fully bonded roofing assemblies," *Construction and Building Materials*, vol. 23, pp. 889-901, 2009.

[18] B. A. Baskaran, S. K. P. Ko, and S. Molleti, "A novel approach to estimate the wind uplift resistance of roofing systems," *Building and Environment*, vol. 44, pp. 723-735, 2009.

[19] S. Molleti, S. K. P. Ko, and B. A. Baskaran, "Effect of fastener-deck strength on the wind-uplift performance of mechanically attached roofing assemblies," *Practice Periodical on Structural Design and Construction*, vol. 15,

no. 1, pp. 27-39, 2010.
[20] R. R. Silva, J. G. Lopes, and J. R. Correia, "The effect of wind suction on flat roofs: An experimental and analytical study of mechanically fastened waterproofing systems," *Construction and Building Materials*, vol. 24, pp. 105-112, 2010.
[21] European Organization for Technical Approvals (EOTA), *Guideline for European technical approval of systems of mechanically fastened flexible roof waterproofing membranes*. EATG 006, Brussel: EOTA, 2000.
[22] A. Baskaran and J. Borujerdi, "Application of numerical models to determine wind uplift ratings of roof," *Wind and Structures*, vol. 4, no. 3, pp. 213-226, 2001.
[23] A. Baskaran and S. Molleti, "Application of numerical models to evaluate wind uplift ratings of roof: Part II," *Wind and Structures*, vol. 8, no. 3, pp. 213-233, 2005.
[24] A. Baskaran, B. Murty, and J. Wu, "Calculating roof membrane deformation under simulated moderate wind uplift pressures," *Engineering Structures*, vol. 31, pp. 642-650, 2009.
[25] D. O. Prevatt, S. D. Schiff, J. S. Stamm, and A. S. Kulkarni, "Wind uplift behavior of mechanically attached single-ply roofing systems: the need for correction factors in standardized tests," *Journal of Structural Engineering*, vol. 134, no. 3, pp. 489-498, 2008.
[26] B. A. Baskaran and O. M. Dutt, "Evaluation of roof fasteners under dynamic wind loading," In Proc. 9th Int. Conf. Wind Eng., New Delhi, India, 1995, pp. 1207-1218.
[27] Architectural Institute of Japan, *Japanese Architectural Standard Specification, JASS 8 Waterproofing and Sealing*. 2014. (in Japanese)
[28] Y. Uematsu, S. Nakamura, and M. Sera, "Evaluation of wind resistant performance of mechanically-attached waterproofing systems in consideration of fatigue damage," In Proc. 20th National Symp. Wind Eng., Tokyo, Japan, 2008, pp. 473-478. (in Japanese)
[29] K. Furuichi, Y. Uematsu, S. Nakamura, and M. Sera, "Evaluation of dynamic wind loads for mechanically-attached waterproofing systems," In Proc. 19th National Symp. Wind Eng., Tokyo, Japan, 2006, pp. 471-476. (in Japanese)
[30] H. Miyauchi, N. Katou, and K. Tanaka, "Force transfer mechanism on fastener section of mechanically anchored waterproofing membrane roofs under wind pressure during typhoons," *Journal of Wind Engineering and Industrial Aerodynamics*, vol. 99, pp. 1174-1183, 2011.
[31] H. Miyauchi, N. Katou, and K. Tanaka, "Behavior of a mechanically anchored waterproofing membrane system under wind suction and uniform pressure," *Building and Environment*, vol. 46, pp. 1047-1055, 2011.
[32] K. Tanaka, D. Chea, T. Lin, N. Kato, and S. Nakamura, "Development of wind resistance test method for mechanically anchored waterproofing membranes," *Journal of Structural and Construction Engineering*, vol. 75, no. 656, pp. 1789-1794, 2010. (in Japanese)
[33] K. Tanaka, S. Ishihara, N. Kato, and H. Miyauchi, "Development of test apparatus for evaluating wind resistance of mechanically anchored waterproofing membrane systems and some results," *Journal of Structural and Construction Engineering*, AIJ, vol. 77, no. 678, pp. 1185-1192, 2012. (in Japanese)
[34] S. Sugiyama, Y. Uematsu, K. Sato, T. Usukura, and K. Ono, "Development of a wind resistance performance test method for mechanically-attached waterproofing systems considering the time-space correlation of wind pressure," *AIJ Journal of Technology and Design*, vol. 25, no. 60, pp. 585-589, 2019. (in Japanese)
[35] G. Lythe and D. Surry, "Wind loading of flat roofs with and without parapets," *Journal of Wind Engineering and Industrial Aerodynamics*, vol. 11, 75-94, 1983.
[36] J. X. Lin, D. Surry, and H.W. Tieleman, "The distribution of pressure near roof corners of flat roof low buildings," *Journal of Wind Engineering and Industrial Aerodynamics*, vol. 56, pp. 235-265, 1995.
[37] J. X. Lin and D. Surry, "The variation of peak loads with tributary area near corners on flat low building roofs," *Journal of Wind Engineering and Industrial Aerodynamics*, vol. 77 & 78, pp. 185-196, 1998.
[38] H. Kawai and G. Nishimura, "Characteristics of fluctuating suction and conical vortices on a flat roof in oblique flow," *Journal of Wind Engineering and Industrial Aerodynamics*, vol. 60, pp. 211-225, 1996.
[39] H. Kawai, "Structure of conical vortices related with suction fluctuation on a flat roof in oblique smooth and turbulent flows," *Journal of Wind Engineering and Industrial Aerodynamics*, vol. 69-71, pp. 579-588, 1997.
[40] Architectural Institute of Japan, *Recommendations for Loads on Buildings*. 2015. (in Japanese)
[41] American Society of Civil Engineers, *Wind Tunnel Testing for Buildings and Other Structures*. ASCE/SEI 49-12, Reston, VA, 2012.
[42] H. Sockel and R. Taucher, "The influence of a parapet on local pressure fluctuations," *Journal of Wind Engineering and Industrial Aerodynamics*, vol. 8, pp. 31-38, 1981.
[43] A. Baskaran and T. Stathopoulos, "Roof corner wind loads and parapet configurations," *Journal of Wind*

*Engineering and Industrial Aerodynamics*, vol. 29, pp. 79-88, 1988.
[44] R. J. Kind, "Worst suctions near edges of flat rooftops with parapets," *Journal of Wind Engineering and Industrial Aerodynamics*, vol. 31, pp. 251-264, 1988.
[45] S. Pindado and J. Meseguer, "Wind tunnel study on the influence of different parapets on the roof pressure distribution of low-rise buildings," *Journal of Wind Engineering and Industrial Aerodynamics*, vol. 91, pp. 1133-1139, 2003.
[46] G. A. Kopp, D. Surry, and C. Mans, "Wind effects of parapets on low buildings: Part 1. Basic aerodynamics and local loads," *Journal of Wind Engineering and Industrial Aerodynamics*, vol. 93, pp. 817-841, 2005.
[47] G. A. Kopp, C. Mans, and D. Surry, "Wind effects of parapets on low buildings: Part 2. Structural loads," *Journal of Wind Engineering and Industrial Aerodynamics*, vol. 93, pp. 843-855, 2005.
[48] C. Mans, G. A. Kopp, and D. Surry, "Wind effects of parapets on low buildings: Part 3. Parapet loads," *Journal of Wind Engineering and Industrial Aerodynamics*, vol. 93, pp. 857-872, 2005.
[49] G. A. Kopp, C. Mans, and D. Surry, "Wind effects of parapets on low buildings: Part 4. Mitigation of corner loads with alternative geometries," *Journal of Wind Engineering and Industrial Aerodynamics*, vol. 93, pp. 873-888, 2005.
[50] W. Suaris and P. Irwin, "Effect of roof-edge parapets on mitigating extreme roof suctions," *Journal of Wind Engineering and Industrial Aerodynamics*, vol. 98, pp. 483-491, 2010.
[51] G. A. Kopp, M. J. Morrison, E. Gavanski, D. J. Henderson, and H. P. Hong, "'Three Little Pigs' Project: Hurricane risk mitigation by integrated wind tunnel and full-scale laboratory tests," *Natural Hazard Review*, pp. 151-161, 2010.
[52] E. Gavanski, M. Takahashi, Y. Uematsu, and M. J. Morrison, "Quantitative performance evaluation of time-varying wind pressure loading actuator," *AIJ Journal of Technology and Design*, vol. 21, no. 49, pp. 1075-1080, 2015. (in Japanese)
[53] E. Gavanski, M. Takahashi, and Y. Uematsu, "Investigation on wind resistance evaluation method of composite sidings with metal," *Journal of Structural and Construction Engineering*, vol. 81, no. 720, pp. 377-383, 2016. (in Japanese)
[54] K. Watanabe and Y. Uematsu, "Evaluation of wind loads on ventilated exterior wall systems," *Journal of Wind Engineering*, vol. 44, no. 2, pp. 23-32, 2019. (in Japanese)
[55] S. Sugiyama, "Development of a wind resistance evaluation method for the mechanically attached waterproofing systems considering the time-space correlation of wind pressures," Master's Thesis, Tohoku University, 2019. (in Japanese)